Tracing Copper−Thiomolybdate Complexes in a Prospective Treatment for Wilson's Disease[†]

Limei Zhang,[‡] Josef Lichtmannegger,[§] Karl H. Summer,[§] Samuel Webb,[||] Ingrid J. Pickering,[‡] and Graham N. George*[,‡]

Department of Geological Sciences, University of Saskatchewan, Saskatoon, Saskatchewan S7N 5E2, Canada, Institute of Toxicology, Helmholtz Zentrum München, German Research Center for Environmental Health (GmbH), Ingolstaedter Landstrasse 1, 85764 Neuherberg, Germany, and Stanford Synchrotron Radiation Laboratory, Stanford Linear Accelerator Center, Menlo Park, California 94025

Received October 14, 2008; Revised Manuscript Received December 17, 2008

ABSTRACT: Wilson's disease is a human genetic disorder which results in copper accumulation in liver and brain. Treatments such as copper chelation therapy or dietary supplementation with zinc can ameliorate the effects of the disease, but if left untreated, it results in hepatitis, neurological complications, and death. Tetrathiomolybdate (TTM) is a promising new treatment for Wilson's disease which has been demonstrated both in an animal model and in clinical trials. X-ray absorption spectroscopy suggests that TTM acts as a novel copper chelator, forming a complex with accumulated copper in liver. We have used X-ray absorption spectroscopy and X-ray fluorescence imaging to trace the molecular form and distribution of the complex in liver and kidney of an animal model of human Wilson's disease. Our work allows new insights into metabolism of the metal complex in the diseased state.

Wilson's disease (*1*) is a human illness in which large quantities of copper accumulate in various organs, including the brain and the liver. It is an autosomal recessive disorder arising from a mutation in the *Atp7b* gene, which codes for a copper-transporting P-type ATPase involved in cellular copper excretion (*2*−*6*). Treatments such as copper chelation therapy or dietary supplementation with zinc can ameliorate the effects of the disease, but if left untreated, it results in hepatitis, neurological complications, and death (*7*−*11*). The exact symptoms vary from patient to patient, and individuals can present chronic hepatitis or acute liver failure and neurological and psychiatric symptoms (*7*−*11*).

Long−Evans cinnamon (LEC) rats carry a deletion in the *Atp7b* gene and have been a widely used animal model for Wilson's disease (*12, 13*). An alternative product known as pineal night-specific ATPase (PINA)[1] is generated by an intronic promoter in the *Atp7b* gene, a putative Cu transporter expressed in pineal gland and in retina which is also defective in LEC rats (*14*). Recently, it has been shown that LEC rats contain an additional defect in serotonin *N*-acetyltransferase (NAT), the key enzyme in melatonin production (*14*). Ahmed et al. have obtained a new strain of rat that is defective only in the PINA/Atp7b locus by crossing LEC rats with normal rats (*14*). The new strain, called LPP rat, represents an improved animal model for Wilson's disease.

Current drug treatments for Wilson's disease can be divided into two strategies, Zn^{2+} administration and copper chelation therapy. Administration of Zn^{2+} is thought to be effective by inducing intestinal metallothionein which may partially block copper absorption and by inducing tissue metallothioneins which may serve to reduce the toxic effects of copper (*15*). Chelation therapy (*16*) is thought to mobilize excess copper for excretion, and prescription-approved drugs currently include D-penicillamine (drug names Cuprimine and Depen) and triethylenetetramine (trientine). Both of these drugs are expected to effectively bind Cu^{2+} although no structurally characterized compounds have yet been prepared (*17*). Furthermore, both drugs exhibit unwanted side effects, and long-term neurological deterioration is also observed (*18*). Tetrathiomolybdate (TTM, $[MoS_4]^{2-}$) is a promising new treatment for Wilson's disease (*19*−*21*), which appears to act by effectively chelating copper to form clusters (*16, 22*). Thus, in our earlier work, we used X-ray absorption spectroscopy (XAS) to identify a Cu−Mo multimetallic cluster in lysosomal extracts of TTM-treated LEC rats (*22*). As previously discussed, TTM can potentially bind up to six copper ions (*16, 22*), possibly allowing it to remove copper rather more efficiently than currently used copper chelators. Furthermore, clinical trial data are highly encouraging; in both open-labeled and randomized controlled double-blind tests, TTM showed less than 5% neurological

[†] This work was supported by grants from the Canadian Institutes of Health Research and the Natural Sciences and Engineering Research Council Canada and by Canada Research Chair awards (G.N.G. and I.J.P.). X-ray fluorescence imaging and X-ray absorption spectra were collected at the Stanford Synchrotron Radiation Laboratory, which is funded by the U.S. Department of Energy, Offices of Basic Energy Sciences and Biological and Environmental Research, with additional support from the National Institutes of Health, National Center for Research Resources.

* Author to whom correspondence should be addressed: e-mail, g.george@usask.ca; tel, +1-306-966-5722; fax, +1-306-966-8593.

[‡] University of Saskatchewan.

[§] Helmholtz Zentrum München.

[||] Stanford Synchrotron Radiation Laboratory.

[1] Abbreviations: TTM, tetrathiomolybdate; SSRL, Stanford Synchrotron Radiation Laboratory; DFT, density functional theory; XAS, X-ray absorption spectroscopy; XFI, X-ray fluorescence imaging; PINA, pineal night-specific ATPase; NAT, *N*-acetyltransferase.

10.1021/bi801926e CCC: $40.75
Published on Web 01/15/2009

deterioration, compared to 50% for D-penicillamine and more than 20% for trientine (*20, 21*). Despite these successes, open questions still remain. In particular, although we have demonstrated the formation of Cu−TTM complexes in purified preparations of liver lysosomes, *in situ* measurements of whole tissues have not yet been reported. Furthermore, following TTM treatment Mo and Cu appear to accumulate in kidney (*23*), and the mechanisms underlying this accumulation are as yet unclear.

We report herein an extension of our previous work, employing the improved animal model (LPP rat). In our previous XAS work we employed animals repeatedly dosed with TTM (*22*), whereas here we examine the results of a single TTM dose. We use X-ray absorption spectroscopy (XAS) to demonstrate the presence of multimetallic clusters in liver and kidney and use X-ray fluorescence imaging (XFI) to demonstrate colocalization of Cu and Mo in tissues.

MATERIALS AND METHODS

Sample Preparation. LPP rats with *Atp7b*(−/−) of approximately 100 days in age were observed to be jaundiced (characteristic of liver dysfunction). Ten milligrams of TTM/kg of body weight was administered as previously described (*24*) 4 days before sample collection. Analysis of serum aspartate aminotransferase and bilirubin was performed as previously described (*24*). Control animals were *Atp7b*(+/−) and appeared healthy with normal levels of serum aspartate aminotransferase bilirubin and liver copper. Animals were exsanguinated under ether anesthesia and samples taken. Samples were additionally taken from *Atp7b*(−/−) LPP rats but without TTM treatment. For the tissue section imaging samples were fixed in 4% neutral formalin and then embedded in 20% gelatin. Sections of 10 μm for high-resolution scans were fixed in 4% paraformaldehyde for 2 h at room temperature and then were dehydrated in a gradient series (0%, 25%, 50%, 75%, and 100%) of ethanol in PBST buffer (30 mM PBS, 0.1% Tween 20) for 5 min each. The fixed and dehydrated sections were then rehydrated in PBST by 5 min washes in the above ethanol gradient in the reverse order. The rehydrated sections were then infiltrated in JB-4 polymer solution (Polysciences Inc., Warrington, PA) for approximately 20 h at 4 °C, with one change of solution, and then left overnight to polymerize. Sections with 10 μm thickness were prepared on a microtome using glass knives. Of two adjacent sections, one was mounted on a glass slide and stained with methylene blue, while the other, intended for XFI high-resolution scan, was fixed on a Thermanox plastic coverslip (Gibco BRL) without any further processing.

For X-ray absorption spectroscopy, the whole fresh liver or kidney was sliced and packed into 2 mm Lucite sample holders with Mylar windows and kept frozen in liquid nitrogen prior to data acquisition.

X-ray Fluorescence Imaging and Data Analysis. Rapid XFI (50 μm resolution) and high-resolution XFI (2.5 μm × 3.5 μm resolution) measurements were conducted at the Stanford Synchrotron Radiation Laboratory (SSRL) on beamlines 6-2 and 2-3, respectively, as previously described (*25, 26*). Incident X-ray energies of 13 and 20.5 keV were used for 6-2 and 9-3, respectively, with the sample at 45° to the incident X-ray beam. X-ray fluorescence was monitored using a silcon-drift vortex detector (SII NanoTechnology USA Inc.) set in the plane of the beam path at 90° to the incident beam and 45° to the sample. Elemental mapping was achieved and corrected for scatter as previously described (*27*). Effective count times were 6.7 ms and 4 s per pixel for rapid and high-resolution XFI, respectively.

X-ray Absorption Spectroscopy Data Acquisition. Cu and Mo K-edge XAS data were collected on beamline 7-3 at SSRL employing a Si(220) double-crystal monochromator. Harmonic rejection at the Cu K-edge was accomplished by adjusting the cutoff of a Rh-coated vertical collimating mirror to 15 keV, whereas for Mo K-edge measurements the collimating mirror was removed, and harmonic rejection was achieved by detuning the second monochromator crystal to 50% of peak intensity. The incident and transmitted X-ray intensities were monitored using ionization chambers filled with either nitrogen (for Cu) or argon (for Mo). X-ray absorption was measured as either Cu or Mo Kα fluorescence excitation spectrum using an array of 30 germanium detectors (*28*). During data collection, samples were maintained at a temperature of approximately 10 K using an Oxford instruments liquid helium flow cryostat. For each sample, eight to ten 35 min scans for Cu K-edge data or four 40 min scans for Mo K-edge data were averaged. X-ray energy was calibrated by reference to the absorption of a Cu or Mo standard metal foil measured simultaneously with each scan, assuming a lowest energy inflection point of 8980.3 or 20003.9 eV for Cu or Mo, respectively.

X-ray Absorption Spectroscopy Data Analysis. The extended X-ray absorption fine structure (EXAFS) oscillations $\chi(k)$ were quantitatively analyzed by k-space curve fitting using the EXAFSPAK suite of computer programs (http://ssrl.slac.stanford.edu/exafspak.html). *Ab initio* theoretical phase and amplitude functions were calculated using the program FEFF version 8.25 (*29*). No smoothing, filtering, or related operations were performed on the data.

Metal Analysis. Metal stoichiometries were determined by inductively coupled plasma mass spectroscopy (ICP-MS). The liver or kidney tissues were measured by wet weight and digested with 69% nitric acid (from EMD Chemicals, catalog no. NX0409-52) and 30% hydrogen peroxide solution (from VWR, catalog no. VW3742-1).

Molecular Modeling. Density functional theory (DFT) molecular modeling used the program DMol^3 (*30, 31*) Materials Studio Version 4.1. Using this level of theory, we expect bond length accuracies of around 0.05 Å and good estimates of energetic trends between postulated molecular entities. The Becke exchange (*32*) and Perdew correlation functionals were used to calculate both the potential during the self-consistent field procedure and the energy. Double numerical basis sets included polarization functions for all atoms. Calculations were spin-unrestricted, and all electron relativistic core potentials were used. No symmetry constraints were applied, and optimized geometries used energy tolerances of 2.0×10^{-5} Hartree. The effects of solvation were simulated by using the conductor-like screening model (COSMO) (*33*) employing the dielectric constant of water.

RESULTS AND DISCUSSION

As expected from previous work (*24*) LPP rats developed symptoms consistent with Wilson's disease, exhibiting acute hepatitis at an age of approximately 100 days. Thus, LPP

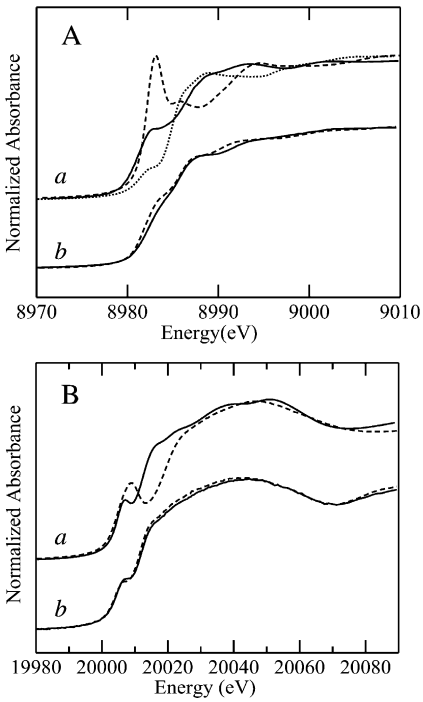

FIGURE 1: (A) Cu K near-edge X-ray absorption spectra. (*a*) shows the spectra of model compounds with different coordination numbers: 2, (•••) $[Cu(SC_{10}H_{12})_2]^-$; 3, (—) $[Cu_4(SPh)_6]^{2-}$; 4, (---) *D. gigas* orange protein $[S_2MoS_2CuS_2MoS_2]^{3-}$ (*34*). (*b*) compares the spectra obtained from TTM-treated LPP rat liver (---) and kidney (—). (B) Mo K near-edge X-ray absorption spectra. (*a*) compares the spectrum of tetrathiomolybdate (—) $[MoS_4]^{2-}$ and molybdate (---) $[MoO_4]^{2-}$, and (*b*) compares the spectra obtained from TTM-treated LPP rat liver (---) and kidney (—).

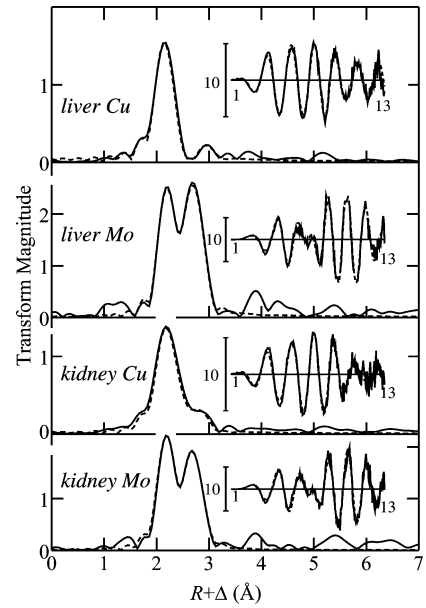

FIGURE 2: Mo and Cu K-edge EXAFS spectra (insets) and EXAFS Fourier transforms of liver and kidney from LPP rat treated with TTM. Fourier transforms are phase-corrected for sulfur backscattering (this gives rise to slight relative shifts between the outer shell peaks of Cu and Mo data sets). Both experimental data (—) and best fits (---) are shown, with the latter computed with the parameters given in Table 1.

rats showed elevated serum aspartate aminotransferase activity and serum bilirubin levels (*24*). Four days after treatment with TTM, LPP rats showed serum aspartate aminotransferase activity and serum bilirubin levels that had reduced to either normal levels or marginally higher than normal levels.

Figure 1a shows the near-edge portion of the Cu K-edge X-ray absorption spectra of kidney and liver from LPP rat treated with a single dose of TTM compared with the spectra of cuprous thiolate standard compounds. None of the Cu near-edge spectra show any signs of the small 1s → 3d transition at ~8979.5 eV characteristic of Cu^{2+}, confirming that copper is predominantly in the cuprous oxidation state (*22*). The feature located around 8983 eV can be assigned as a 1s → 4p transition, which is most intense in digonal coordination environments (*35, 36*). By comparing the intensity of this transition with the corresponding feature in model compound spectra, we observe that it is intermediate in appearance between the three- and four-coordinate Cu^{1+}−S species and that the data are very similar to those reported previously for LEC rat purified liver lysosomes (*22*). Figure 1b shows the Mo K-edge near-edge spectra of liver and kidney from TTM-treated LPP rats. The spectrum can be seen to be very similar to that of tetrathiomolybdate, suggesting a tetrahedral geometry for Mo and a full complement of four sulfur donors. As was the case for Cu, the Mo K-edge spectra are also very similar to those reported previously of purified LEC rat liver lysosomes (*22*).

More structural detail is available from quantitative analysis of the EXAFS portion of the spectrum. Figure 2 shows the Cu and Mo EXAFS and best fits, together with the corresponding EXAFS Fourier transforms, for TTM-treated LPP rats. The EXAFS curve-fitting analysis is summarized in Table 1. All data sets have prominent EXAFS from directly coordinated ligands, which are identified by curve fitting as sulfur. We note in passing that EXAFS cannot readily distinguish between backscatterers of similar atomic number (cf. ref (*37*)); thus EXAFS from S and Cl backscatterers cannot easily be distinguished, whereas S and O are quite straightforward to discriminate. Here we assume the presence of sulfur donors, as these are physiologically far more likely than the alternatives (i.e., phosphorus or chlorine). In addition to first coordination shell sulfurs, the Mo and, to a lesser extent, the Cu EXAFS show clear indications of metal−metal backscattering, indicating the presence of multimetallic clusters. Quantitative curve-fitting analysis indicates that for both liver and kidney Mo is coordinated by four sulfurs at a distance of 2.24 Å while Cu is coordinated by between three and four sulfurs at 2.27−2.28 Å (Table 1). This is as expected from the near-edge spectra (discussed above).

Metal−metal EXAFS is observed for both Cu and Mo but is more pronounced for Mo, and we will therefore discuss the Mo case first. Curve fitting of the Mo EXAFS clearly indicates three and four Mo•••Cu interactions at 2.71 and 2.72 Å for kidney and liver, respectively. This is seen clearly in the EXAFS Fourier transforms as the intense peak at about 2.7 Å. For Cu, however, only a rather low-intensity peak is observed. Similar spectra were observed for purified LEC rat liver lysosomes (*22*). Chemical analysis of the samples yielded Cu:Mo molar stoichiometries of 11.3:1 and 4.3:1 for liver and kidney, respectively. This indicates that liver has considerable additional copper that is not involved in a multimetallic cluster. We therefore examined the Cu K near-edge and EXAFS of LPP rat liver in the absence of TTM treatment (Figure 3). The data indicate a copper environment

Table 1: EXAFS Curve-Fitting Parameters of Kidney and Liver from TTM-Treated and Untreated LPP *Atp7b* (−/−) Rats[a]

	Mo−S			Mo···Cu			
treated	*N*	*R*	σ^2	*N*	*R*	σ^2	*F*
kidney	4	2.237 (3)	0.0034 (1)	3	2.706 (3)	0.0037 (1)	0.261
liver	4	2.245 (2)	0.0025 (1)	4	2.721 (2)	0.0035 (1)	0.251

	Cu−S			Cu···Mo			Cu···Cu			
treated	*N*	*R*	σ^2	*N*	*R*	σ^2	*N*	*R*	σ^2	*F*
kidney	3.6 (1)	2.280 (3)	0.0069 (3)	0.5 (3)	2.706[b]	0.0037[b]				0.269
liver	3	2.265 (2)	0.0049 (1)	0.4 (1)	2.721[b]	0.0035[b]	1.1 (1)[c]	2.698[d]	0.0088[d]	0.227
							0.6 (1)[c]	2.878[d]	0.0091[d]	

	Cu−S			Cu···Cu			
untreated	*N*	*R*	σ^2	*N*	*R*	σ^2	*F*
liver	3	2.253 (2)	0.0045 (1)	2	2.698 (5)	0.0088 (4)	0.273
				1	2.878 (11)	0.0091 (4)	

[a] Coordination numbers *N*, interatomic distances *R* (Å), and Debye−Waller factors σ^2 (Å^2). Values in parentheses are the estimated standard deviations (precisions) obtained from the diagonal elements of the covariance matrix. The accuracies will be much greater than these values and are generally accepted to be ±0.02 Å for bond lengths and ±20% for coordination numbers and Debye−Waller factors. The fit-error function *F* is defined as $F = [\sum k^6(\chi_{calc} - \chi_{expt})^2/\sum\chi_{expt}^2]^{1/2}$, where the summations are over all data points included in the refinement. [b] Value fixed to that determined from Mo K-edge EXAFS curve fitting. [c] The ratio of the Cu···Cu *N* values was held fixed at the 2:1 value used to model the untreated LPP rat Cu K-edge EXAFS. [d] Value fixed at that determined from fitting untreated LPP rat *Atp7b* (−/−) Cu K-edge EXAFS (untreated, liver).

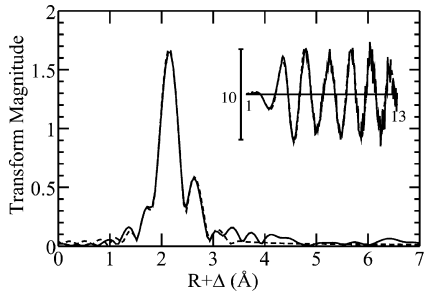

FIGURE 3: Cu K-edge EXAFS spectra (inset) and EXAFS Fourier transforms of liver from untreated LPP rat. Fourier transforms are phase-corrected for sulfur backscattering. Both experimental data (—) and best fits (---) are shown, with the latter computed with the parameters given in Table 1.

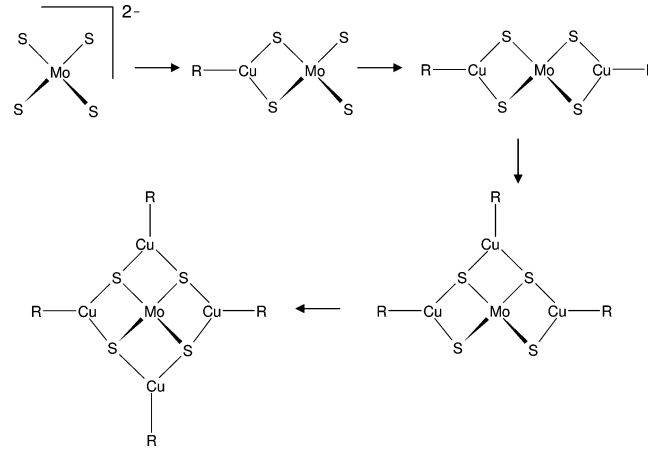

FIGURE 4: Schematic diagram of formation of polymetallic clusters by sequential addition of copper moieties to tetrathiomolybdate.

that is very similar to that of copper metallothionein (*38*) with mostly trigonal Cu−S coordination (Cu−S 2.25 Å) plus a weaker Cu···Cu at about 2.7 Å. This is in agreement with previous work indicating that copper in LEC rat liver is predominantly bound by metallothioneins (*24*). The Cu···Cu interaction was modeled for simplicity with only two partially canceling Cu···Cu components (Table 1), but we note that Cu methallothionein will be expected to have rather more components (e.g., the yeast protein has up to 10 different Cu···Cu interactions) which will interfere with each other and will partially cancel (*38*). Thus, the current data on copper in TTM-treated LPP rat liver will represent the sum of the spectrum of copper that is not involved in Cu−Mo complexes with that of the Cu−Mo complexes. We note that the ~2.7 Å Cu···Cu EXAFS will effectively cancel EXAFS from Cu···Mo as EXAFS from Mo and Cu backcatterers are expected to be 180° out of phase, with Mo having higher amplitude than Cu especially at higher *k*, all other factors being equal. EXAFS cancelation is discussed in more detail by George (*39*) and by Zhang et al. (*38*). Because of this complexity the Cu EXAFS from TTM-treated LPP rat liver was modeled by taking the parameters for the Cu···Cu interaction from the analysis of untreated LPP rat liver (Table 1, Figure 3), keeping these fixed, and using the Cu···Mo parameters from the Mo K-edge curve-fitting analysis, allowing only the combined Cu···Cu amplitude and the Cu···Mo amplitude to refine. If these parameters were freely floated, then similar bond lengths and Debye−Waller factors were obtained, except that very high (undesirable) correlations between parameters were found upon examination of the covariance matrix.

In contrast to the situation with liver, for kidney the elemental stoichiometry is much closer to that observed by Mo K-edge EXAFS (3:1), suggesting that much of the copper present is involved in Cu−Mo complexes.

The chemistry of copper−molybdenum−sulfur clusters has been extensively investigated. A rich chemistry exists, much of which involving multimetallic clusters where Cu and Mo are arranged in rhombs involving two bridging sulfurs. Tetrathiomolybdate tends to form species bridged to individual cuprous ions by two of its four sulfur ligands, so that the copper bridges across one edge of the tetrahedron of sulfur atoms. Complexes with Cu:Mo stoichiometries of 1 through 6 have been structurally characterized, with 3 being the most common, and 4 a close second (*17*). Figure 4 illustrates the sequential addition of copper to tetrathiomolybdate, up to a Cu:Mo stoichiometry of 4 (i.e., stoichiom-

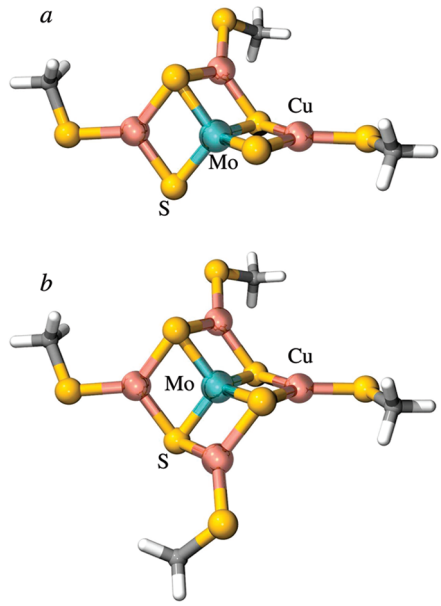

FIGURE 5: Density functional theory energy-minimized structures for (*a*) $[(CH_3SCu)_3MoS_4]^{2-}$ and (*b*) $[(CH_3SCu)_4MoS_4]^{2-}$. For (*a*) selected computed average interatomic distances were Cu−SCH_3 2.217 Å, Cu−S(bridging) 2.270 Å, Mo−S 2.283 Å, Cu···Mo 2.702 Å, and Cu···Cu 3.760 Å. For (*b*) selected computed average interatomic distances are Cu−SCH_3 2.214 Å, Cu−S(bridging) 2.291 Å, Mo−S 2.297 Å, Cu···Mo 2.703 Å, and Cu···Cu 3.821 Å.

etries 5 and 6 are not illustrated). Energy-minimized structures of idealized $[(CuSR)_3MoS_4]^{2-}$ and $[(CuSR)_4MoS_4]^{2-}$ clusters are shown in Figure 5. The computed bond lengths (see caption to Figure 5) agree very well both with values from the Cambridge Crystallographic Database (*17*) and with those obtained from EXAFS (Table 1). Thus, our results are consistent with a mechanism in which copper is effectively chelated by thiomolybdate in liver (Figure 4), and the resulting complexes are then at least in part mobilized to kidney. The nature of the external ligands to copper is worth addressing and may be relevant to transport. The EXAFS data indicate that these are sulfur ligands, with chloride being a rather less likely alternative. Given that the copper−molybdenum species are at least fractionally mobilized, a likely candidate for the external ligands to copper of those clusters that are mobilized is glutathione. Glutathione is the most prevalent intracellular thiol in higher eukaryotes, and its association with a Cu−Mo cluster might allow transport via one of the glutathione-linked transporters (e.g., ref (*40*)) facilitating transport from the liver and eventual localization to kidney.

The mobilization of Cu to kidney prompted us to investigate its localization further using X-ray fluorescence imaging (XFI). Samples were studied at two different spatial resolutions: macroscopic maps of sections of whole kidney employing a pixel size of 50 × 50 μm^2 and microscopic scans with a pixel size of 3.5 μm (h) × 2.5 μm (v). For the former resolution, Mo localizations could not be included in the maps since the maximum beamline energy was below the Mo K-edge. Mo L-edge fluorescence also cannot be used because of overlap of the Mo L fluorescence lines with the intense sulfur K-edge fluorescence due to the high sulfur content of biological samples. Figure 6 shows the distribution of Cu in a longitudinal section of TTM treated LPP rat kidney. Marked accumulation of copper is observed in the cortex of the kidney, at levels that are approximately 4 times

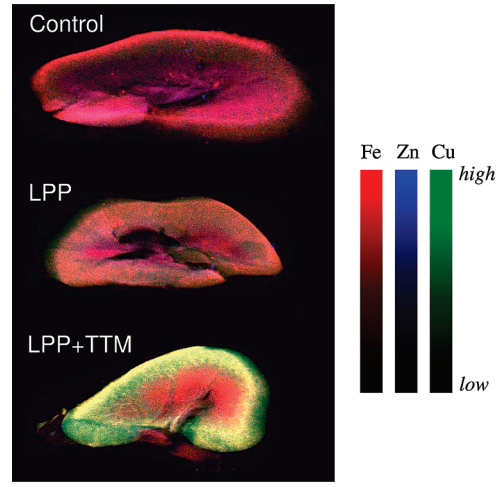

FIGURE 6: XFI maps of kidney, showing Fe, Zn, and Cu levels (arbitrary scales) as red, blue, and green, respectively. The maps shown are as follows: control, kidney from LPP rat *Atp7b* (+/−), no jaundice; LPP, LPP rats *Atp7b* (−/−), jaundiced but no TTM treatment; LPP + TTM, LPP rats *Atp7b* (−/−), jaundiced and TTM-treated.

that found in jaundiced LPP rats with no TTM treatment (Figure 6). In contrast, Cu levels in kidney medulla were comparable in LPP rats with and without TTM treatment. No significant changes in the distributions of other metals, such as Fe and Zn, were observed, apart from a slight decrease in cortex iron with both treated and untreated LPP rats (Figure 6).

Microscopic sections of kidney cortex (10 μm thick) of TTM-treated LPP rat were examined at the higher X-ray resolution of 3.5 μm (h) × 2.5 μm (v). Figure 7 shows a representative image with X-ray fluorescence imaging maps of both Cu and Mo and an optical micrograph of the corresponding (adjacent) section stained with methylene blue. In general, the Mo and Cu X-ray fluorescence intensities show a high degree of correlation (Pearson product-moment correlation coefficient = 0.86), which is consistent with the conclusions from bulk XAS that the bulk of Cu and Mo present is covalently associated in a multimetallic cluster. Comparison of the optical micrograph, the well-known anatomy of the kidney tubule, and the XFI maps (Figure 7) indicates that Cu and Mo accumulate in the proximal convoluted tubules but not in the glomeruli or in the distal convoluted tubules. This cell-specific colocalization of Cu and Mo suggests that the Cu and Mo are released from the blood into the filtrate in the glomerulus cavity and then reabsorbed and accumulated locally when passing through the proximal tubules. This reabsorption by the proximal tubules provides an explanation for the accumulation of Cu and Mo within the kidney cortex.

Ogra et al. have suggested that the Cu−TTM complexes that form in liver can be divided into soluble and insoluble and fractions and that the latter might be slowly dissolved and subsequently excreted (*41*). From the XAS perspective the copper−molybdenum clusters that form in liver are structurally similar to those in kidney, and the difference may simply be the nature of the external thiolate ligands to copper, as we have discussed above. How TTM abstracts Cu from metallothionein in the liver still remains to be clarified. In fully loaded copper metallothionein a proportion of the copper is more loosely bound with digonal two-

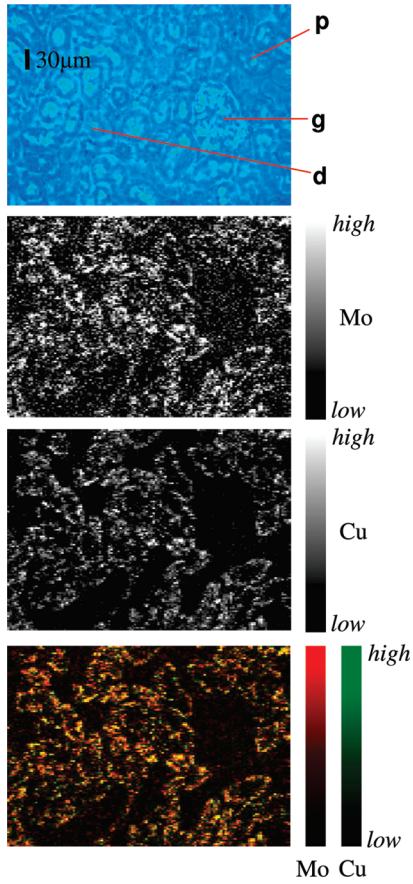

FIGURE 7: XFI of kidney cortex from LPP rat treated with TTM with optical micrograph (top) showing locations of proximal convoluted tubule p, distal convoluted tubule d, and glomerulus g. The similarity of the Mo and Cu XFI maps is evident. A combined Cu and Mo map showing Cu in green and Mo in red is shown in the lower panel.

coordinate cuprous thiolate (*38*). We have conducted preliminary DFT calculations (not illustrated) that indicate that TTM should be able to sequester this copper by providing an additional sulfur ligand and then by partially abstracting the copper from its metallothionein binding site by forming MoS_2Cu rhombs. We also note that hepatitis is unlikely to be caused by Cu when it is actually bound to metallothionein, and perhaps it is the small fraction of free copper ions which is scavenged by TTM. In time, and with equilibration, this scavenging might result in the complexation of a significant fraction of the total copper present.

Finally, the long-term effects of TTM treatment are presently unknown. Haywood et al. (*42*) have reported long-term adverse effects in a flock of copper-poisoned sheep following treatment with TTM which was successful in the short term. However, this study employed quite high oral doses of copper, and it is possible that the physiological fate would differ in a Wilson's patient. Long-term experiments with LPP rat are needed to understand the effects of longer term treatments with TTM. TTM remains a highly promising candidate drug for treatment of Wilson's disease. A molecular understanding of the metallophysiology is vital to its eventual use in a clinical setting, and possible future strategies might involve both TTM and a second copper chelator, possibly customized for metal binding (*43*).

ACKNOWLEDGMENT

We thank Dr. Jimo Borjigin at the University of Michigan (Ann Arbor, MI) for kindly supplying breeding pairs of LPP rats. We also thank Dr. Helen Nichol and members of her research group at the University of Saskatchewan for invaluable help with preparation of microscopic sections and members of the George/Pickering groups and the staff of SSRL for assistance in conducting experiments there.

REFERENCES

1. Wilson, S. A. K. (1912) Progressive lenticular degeneration. A familial nervous disease associated with cirrhosis of the liver. *Lancet 1*, 1115–1119.
2. Bull, P. C., Thomas, G. R., Rommens, J. M., Forbes, J. R., and Cox, D. W. (1993) The Wilson disease gene is a putative copper transporting P-type ATPase similar to the Menkes gene. *Nat. Genet. 5*, 327–337.
3. Petrukhin, K., Fischer, S. G., Pirastu, M., Tanzi, R. E., Chernov, I., Devoto, M., Brzustowicz, L. M., Cayanis, E., Vitale, E., Russo, J. J., Matseoane, D., Boukhgalter, B., Wasco, W., Figus, A. L., Loudianos, J., Cao, A., Sternlieb, I., Evgrafov, O., Parano, E., Pavone, L., Warburton, D., Ott, J., Penchaszadeh, G. K., Scheinberg, I. H., and Gilliam, T. C. (1993) Mapping, cloning and genetic-characterization of the region containing the Wilson disease gene. *Nat. Genet. 5*, 338–343.
4. Tanzi, R. E., Petrukhin, K., Chernov, I., Pellequer, J. L., Wasco, W., Ross, B., Romano, D. M., Parano, E., Pavone, L., Brzustowicz, L. M., Devoto, M., Peppercorn, J., Bush, A. I., Sternlieb, I., Pirastu, M., Gusella, J. F., Evgrafov, O., Penchaszadeh, G. K., Honig, B., Edelman, I. S., Soares, M. B., Scheinberg, I. H., and Gilliam, T. C. (1993) The Wilson disease gene is a copper transporting ATPase with homology to the Menkes disease gene. *Nat. Genet. 5*, 344–350.
5. Yamaguchi, Y., Heiny, M. E., and Gitlin, J. D. (1993) Isolation and characterization of a human liver cDNA as a candidate gene for Wilson disease. *Biochem. Biophys. Res. Commun. 197*, 271–277.
6. Roelofsen, H., Wolters, H., Van Luyn, M. J. A., Miura, N., Kuipers, F., and Vonk, R. J. (2000) Copper-induced apical trafficking of ATP7B in polarized hepatoma cells provides a mechanism for biliary copper excretion. *Gastroenterology 119*, 782–793.
7. Fink, J. K., Hedera, P., and Brewer, G. J. (1999) Hepatolenticular degeneration (Wilson's disease). *Neurologist 5*, 171–185.
8. Loudianos, G., and Gitlin, J. D. (2000) Wilson's disease. *Semin. Liver Dis. 20*, 353–364.
9. Walshe, J. A. (2006) History of Wilson's disease: 1912 to 2000. *Movement Disord. 21*, 142–147.
10. Ala, A., Walker, A. P., Ashkan, K., Dooley, J. S., and Schilsky, M. L. (2007) Wilson's disease. *Lancet 369*, 397–408.
11. Pfeiffer, R. F. (2007) Wilson's disease. *Semin. Neurol. 27*, 123–132.
12. Li, Y., Togashi, Y., Sato, S., Emoto, T., Kang, J. H., Takeichi, N., Kobayashi, H., Kojima, Y., Une, Y., and Uchino, J. (1991) Spontaneous hepatic copper accumulation in Long-Evans Cinnamon rats with hereditary hepatitis. A model of Wilson's disease. *J. Clin. Invest. 87*, 1858–1861.
13. Wu, J., Forbes, J. R., Chen, H. S., and Cox, D. W. (1994) The LEC rat has a deletion in the copper transporting ATPase gene homologous to the Wilson disease gene. *Nat. Genet. 7*, 541–545.
14. Ahmed, S., Deng, H., and Borjigin, J. (2005) A new strain of rat for functional analysis of PINA. *Mol. Brain Res. 137*, 63–69.
15. Yuzbasiyangurkan, V., Grider, A., Nostrant, T., Cousins, R. J., and Brewer, G. J. (1992) Treatment of Wilson's disease with zinc. 10. Intestinal metallothionein induction. *J. Lab. Clin. Med. 120*, 380–386.
16. George, G. N., Pickering, I. J., Doonan, C. J., Korbas, M., Singh, S. P, and Hoffmeyer, R. (2008) Inorganic molecular toxicology and chelation therapy of heavy metals and metalloids. *Adv. Mol. Toxicol. 2*, 125–155.
17. Allen, F. H., and Kennard, O. (1983) The Cambridge database of molecular structures. *Perspect. Comput. 3*, 28–43.
18. Brewer, G. J., Terry, C. A., Aisen, A. M., and Hill, G. M. (1987) Worsening of neurologic syndrome in patients with Wilson's disease with initial penicillamine therapy. *Arch. Neurol. 44*, 490–493.

19. Brewer, G. J., Dick, R. D., Yuzbasiyangurkin, V., Tankanow, R., Young, A. B., and Kluin, K. J. (1991) Initial therapy of patients with Wilson's disease with tetrathiomolybdate. *Arch. Neurol. 48*, 42–47.
20. Brewer, G. J., Hedera, P., Kluin, K. J., Carlson, M., Askari, F., Dick, R. B., Sitterly, J., and Fink, J. K. (2003) Treatment of Wilson disease with ammonium tetrathiomolybdate: III. Initial therapy in a total of 55 neurologically affected patients and follow-up with zinc therapy. *Arch. Neurol. 60*, 379–385.
21. Brewer, G. J., Askari, F., Lorincz, M. T., Carlson, M., Schilsky, M., Kluin, K. J., Hedera, P., Moretti, P., Fink, J. K., Tankanow, R., Dick, R. B., and Sitterly, J. (2006) Treatment of Wilson disease with ammonium tetrathiomolybdate: IV. Comparison of tetrathiomolybdate and trientine in a double-blind study of treatment of the neurologic presentation of Wilson disease. *Arch. Neurol. 63*, 521–527.
22. George, G. N., Pickering, I. J., Harris, H. H., Gailer, J., Klein, D., Lichtmannegger, J., and Summer, K. H. (2003) Tetrathiomolybdate causes formation of hepatic copper-molybdenum clusters in an animal model of Wilson's disease. *J. Am. Chem. Soc. 125*, 1704–1705.
23. Komatsu, Y., Sadakata, I., Ogra, Y., and Suzuki, K. T. (2000) Excretion of copper complexed with thiomolybdate into the bile and blood in LEC rats. *Chem.-Biol. Interact. 124*, 217–231.
24. Klein, D., Arora, U., Lichtmannegger, J., Finckh, M., Heinzmann, U., and Summer, K. H. (2004) Tetrathiomolybdate in the treatment of acute hepatitis in an animal model for Wilson disease. *J. Hepatol. 40*, 409–416.
25. Popescu, B. F. G., Belak, Z. R., Ignatyev, K., Ovsenek, N., and Nichol, H. (2007) Asymmetric distribution of metals in the *Xenopus laevis* oocyte: a synchrotron X-ray fluorescence microprobe study. *Biochem. Cell. Biol. 85*, 537–542.
26. Korbas, M., Blechinger, S., Krone, P. H., Pickering, I. J., and George, G. N. (2008) Organomercury uptake in zebrafish larvae. *Proc. Natl. Acad. Sci. U.S.A. 105*, 12108–12112.
27. Pickering, I. J., Prince, R. C., Salt, D. E., and George, G. N. (2000) Quantitative chemically-specific imaging of selenium transformation in plants. *Proc. Natl. Acad. Sci. U.S.A. 97*, 10717–10722.
28. Cramer, S. P., Tench, O., Yocum, M., and George, G. N. (1988) A 13-element Ge detector for fluorescence EXAFS. *Nucl. Instrum. Methods Phys. Res., Sect. A 266*, 586–591.
29. Rehr, J. J., Deleon, J. M., Zabinsky, S. I., and Albers, R. C. (1991) Theoretical X-ray absorption fine-structure standards. *J. Am. Chem. Soc. 113*, 5135–5140.
30. Delley, B. (1990) An all-electron numerical-method for solving the local density functional for polyatomic-molecules. *J. Chem. Phys. 92*, 508–517.
31. Delley, B. (2000) From molecules to solids with the DMol(3) approach. *J. Chem. Phys. 113*, 7756–7764.
32. Becke, A. D. (1988) A multicenter numerical-integration scheme for polyatomic-molecules. *J. Chem. Phys. 88*, 2547–2553.
33. Delley, B. (2006) The conductor-like screening model for polymers and surfaces. *Mol. Simul. 32*, 117–123.
34. George, G. N., Pickering, I. J., Yu, E. Y., Prince, R. C., Bursakov, S. A., Gavel, O. Y., Moura, I., and Moura, J. J. G. (2000) A novel protein-bound copper-molybdenum cluster. *J. Am. Chem. Soc. 132*, 8321–8322.
35. Kau, L. S., Spirasolomon, D. J., Pennerhahn, J. E., Hodgson, K. O., and Solomon, E. I. (1987) X-ray absorption-edge determination of the oxidation-state and coordination-number of copper−Application to the type-3 site in rhus-vernicifera laccase and its reaction with oxygen. *J. Am. Chem. Soc. 109*, 6433–6442.
36. Pickering, I. J., George, G. N., Dameron, C. T., Kurtz, B., Winge, D. R., and Dance, I. G. (1993) X-ray absorption spectroscopy of cuprous-thiolate clusters in proteins and model systems. *J. Am. Chem. Soc. 115*, 9498–9505.
37. George, G. N., and Pickering, I. J. (2007) X-ray absorption spectroscopy in biology and chemistry, in *Brilliant Light in Life and Materials Sciences* (Tsakanov, V., and Wiedemann, H., Eds.) pp 97−119, Springer, Dordrecht, The Netherlands.
38. Zhang, L., Pickering, I. J., Winge, D. R., and George, G. N. (2008) X-ray absorption spectroscopy of cuprous-thiolate clusters in *Saccharomyces cerevisiae* metallothionein. *Chem. Biodivers. 5*, 2042–2049.
39. George, G. N. (1997) X-ray absorption spectroscopy of molybdenum enzymes. *J. Biol. Inorg. Chem. 2*, 790–796.
40. Lee, T.-C., Ho, I.-C., Lu, W.-J., and Huang, J.-D. (2006) Enhanced expression of multidrug resistance-associated protein 2 and reduced expression of aquaglyceroporin 3 in an arsenic-resistant human cell line. *J. Biol. Chem. 281*, 18401–18407.
41. Ogra, Y., Chikusa, H., and Suzuki, K. T. (2000) Metabolic fate of the insoluble copper/tetrathiomolybdate complex formed in the liver of LEC rats with excess tetrathiomolybdate. *J. Inorg. Biochem. 78*, 123–128.
42. Haywood, S., Dincer, Z., Jasani, B., and Loughran, M. J. (2004) Molybdenum-associated pituitary endocrinopathy in sheep treated with ammonium tetrathiomolybdate. *J. Comp. Pathol. 130*, 21–31.
43. George, G. N., Prince, R. C., Gailer, J., Buttigieg, G. A., Denton, M. B., Harris, H. H., and Pickering, I. J. (2004) Mercury binding to the chelation therapy agents DMSA and DMPS, and the rational design of custom chelators for mercury. *Chem. Res. Toxicol. 17*, 999–1006.

BI801926E